



Fermi National Accelerator Laboratory

Fermilab-TM-2398-AD-APC

**The Modeling of Microbunch Injection
into the Main Injector¹**

Phil S. Yoon², David E. Johnson, and Weiren Chou

Fermi National Accelerator Laboratory, Batavia, IL 60510³

January 2008

¹ Typeset by \LaTeX

² E-mail: syoon@fnal.gov

³ Work supported by Fermilab Research Alliance (FRA), LLC under contract No. DE-AC02-07-CH11359 with the United States Department of Energy

Abstract

This technical memo presents the modeling of time-structured multiturn injection for an upgraded Main Injector with the 8-GeV Super-Conducting proton driver, or an ILC-style linac, or a Project-X linac. The Radio-Frequency mismatch between a linac and the upgraded Main Injector will induce parasitic longitudinal painting in RF-phase direction. Several different scenarios with a choice of different RF parameters for single RF system and double RF system in the presence of longitudinal space charge have been investigated. From the studies of microbunch injection with the aid of *ESME (2003)* numerical simulations, it is found that the dual RF system with a choice of appropriate RF parameters allows us to overcome the space-charge limitation set by beam intensity during the multiturn-injection process. A double RF system with a harmonic ratio ($R_H = H_2/H_1$) of 2.0 and a voltage ratio ($R_V = V_2/V_1$) of 0.5 are most favored to reduce both longitudinal and transverse effects of space charge in the Main Injector.

Disclaimer

This report was prepared as an account of work sponsored by an agency of the United States Government. Neither the United States Government nor any agency thereof, nor any of their employees, makes any warranty, expressed or implied, or assumes any legal liability or responsibility for the accuracy, completeness or usefulness of any information, apparatus, product, or process disclosed, or represents that its use would not infringe privately owned rights. Reference herein to any specific commercial product, process, or service by trade name, trademark, manufacturer, or otherwise, does not necessarily constitute or imply its endorsement, recommendation, or favoring by the United States Government or any agency thereof. The views and opinions of authors expressed herein do not necessarily state or reflect those of the United States Government or any agency thereof.

Distribution

Approved for public release; further dissemination unlimited.

Microbunch Injection into the Main Injector

from a superconducting linac into the Main Injector

After studying the method of time-structured multiturn injection from the present 400-MeV linac to Fermilab's Booster [1], we have further explored the method of microbunch injection for applications to the Main Injector: from a future Super-Conducting (SC) linac to an upgraded Main Injector (FMI-2)¹ including parasitic longitudinal painting. The future SC linac referred herein can be the 8-GeV SCRF linac proton driver [2–4], or an ILC-style linac, or the Project-X linac.

Overview of the Main Injector

The Main Injector (MI) is a ring with a circumference of about 3.3 (km). The central roles of the MI is to connect to the Tevatron, the Booster, the Antiproton source, switchyard, and the Recycler ring via a number of beam transport lines in the Fermilab accelerator complex. The MI can accelerate and decelerate particles between 8 GeV and 150 GeV, depending on the mode of operation. The harmonic number of the MI is 588 and harmonic RF at injection is 52.8114 (MHz)²

Overview of the 8-GeV Super-Conducting RF Linac

An 8-GeV SC linac has been proposed as a single-stage H^- injector into the Main Injector as a replacement for the aging 400-MeV Linac and 8-GeV Booster. This would be the highest energy H^- multiturn injection system in the world. Fermilab has been carrying out design studies [4, 5] of the SC linac and injection systems [6] for the last several years. The linac design [7] utilizes a warm-temperature 325-MHz RFQ and rebuncher cavities to bunch the beam at 325 MHz. At $\beta = 0.89$ (about $E_{kin} = 1.1 \text{ GeV}$), the RF of the SC cavities

¹We will use Main Injector (FMI) and upgraded Main Injector (FMI-2) interchangeably herein.

²For the sake of brevity and convenience, MI RF will be referred to as 53 MHz hereafter.

is 1.3 GHz. The ultimate bunch structure required for injection into the MI will be formed by a 325-MHz fast chopper system [8]. The fast chopper system will be required to remove individual 325-MHz bunches or groups of bunches to be matched to the MI RF structure and provide a beam abort notch: two out of every six microbunches³ are to be removed.

Time Structure of the Main Injector

In the injection modeling for the MI with the aid of ESME [9], a train of four microbunches, produced by the fast chopper system located at the front end of the 8-GeV SC RF linac, are injected into the upgraded Main Injector. Figure 1.1 is a schematic illustrating one MI RF bucket that is populated with an initial train of four microbunches. The two chopped microbunches are represented by two consecutive empty 325-MHz RF buckets.

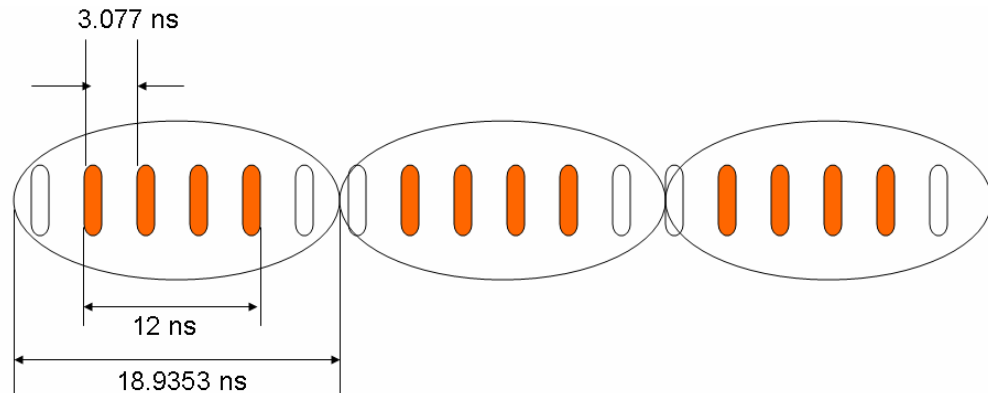


Figure 1.1: Three consecutive MI RF buckets of 53 MHz. A train of four microbunches of 325 MHz are synchronously injected into each standing 53-MHz bucket. Two chopped microbunches are equivalent to 6 ns.

More details of the time structure of the MI RF bucket after the first synchronous injection from a SC linac are illustrated in Figure 1.2.

³The *microbunch* is referred to as a 325-MHz bunch hereafter.

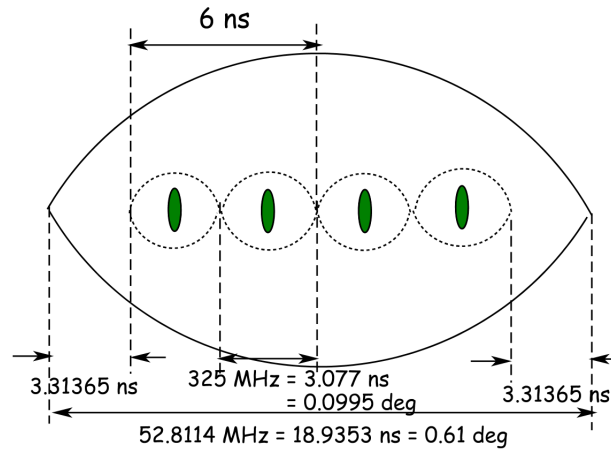


Figure 1.2: The time structure of a single RF system of an upgraded Main Injector: principal RF harmonic of 52.8 (MHz), sub-harmonic of 325 (MHz), and a beam abort notch of 6 ns

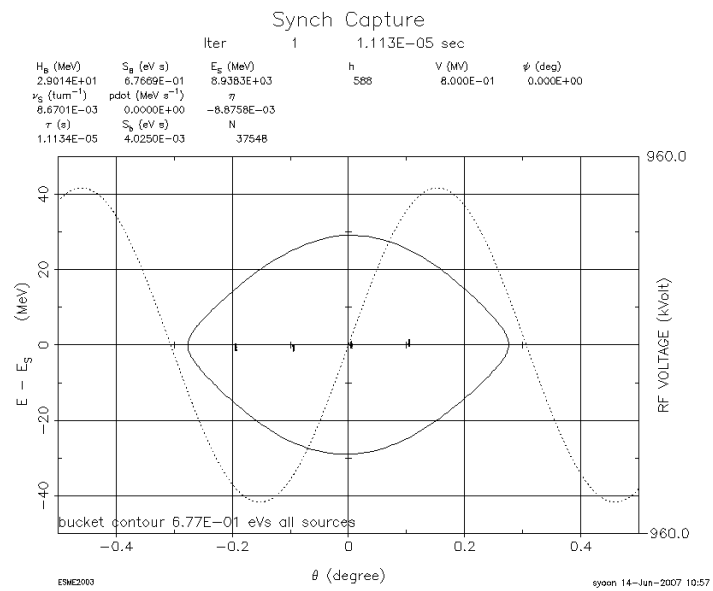


Figure 1.3: Single RF system: the injection of 4 microbunches at the 1st turn with RF waveform drawn in the background

A total beam notch per MI RF bucket is about 6 ns, which corresponds to two 325-MHz RF buckets. Figure 1.3 is a phase-space ($\Delta E, \theta$) plot of the very first train of four microbunches with a RF-voltage waveform drawn in the background. The following is a list of longitudinal parameters that can be found in the header of each ESME phase-space plot in this memo.

iter (number of turns), H_B (bucket height), S_B (bucket area), S_b (bunch area), V (RF voltage), E_s (synchronous energy), v_s (synchrotron tune), $pdot$ (dp/dt), η (slip factor), τ_s (revolution period), h (harmonic number), Ψ (synchronous phase), and N (number of macroparticles)

The horizontal axis is $\Delta\theta$ ($= \theta - \theta_s$) in units of degrees with one full revolution representing 360 (deg), the vertical axis on the left is ΔE ($= E - E_s$) in units of MeV, and the vertical axis on the right is V_{rf} in units of kV for the RF waveform.

The azimuthal-density⁴ and energy-density distribution⁵ of one of four microbunches are plotted in Figures 1.4 and 1.5, respectively. The root-mean-square (RMS) width of one microbunch is 1.96×10^{-4} (deg), which corresponds to 6.05 (ps). The red area indicates the tail portion of a microbunch. The fractional tail portion is about 1.34 %. To make the tail portion of a microbunch stand out, the density distribution is also plotted on a logarithmic scale. The RMS value of *initial* energy spread is about 0.26 (MeV) per each microbunch. Regarding the MI to be a 11.1338- μ s, or 360-degree ring, we used the following conversion factor:

$$0.032335 \text{ (deg/ns)} \tag{1.1}$$

⁴The *azimuthal density* is referred to as the charge density, or the azimuthal profile of macroparticles.

⁵The *energy-density distribution* is referred to as the profile of macroparticles in energy (ΔE) direction.

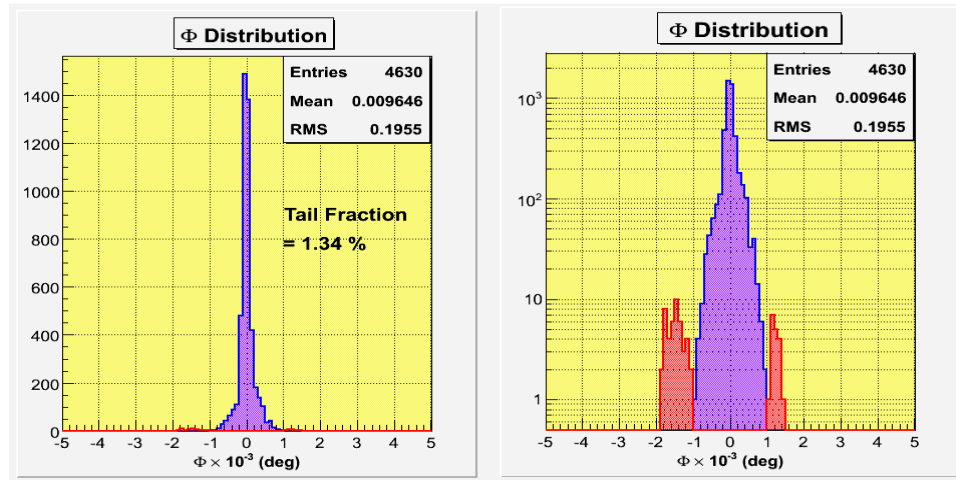


Figure 1.4: Zero-centered charge density with tail portion; (left) on a linear scale (right) on a logarithmic scale

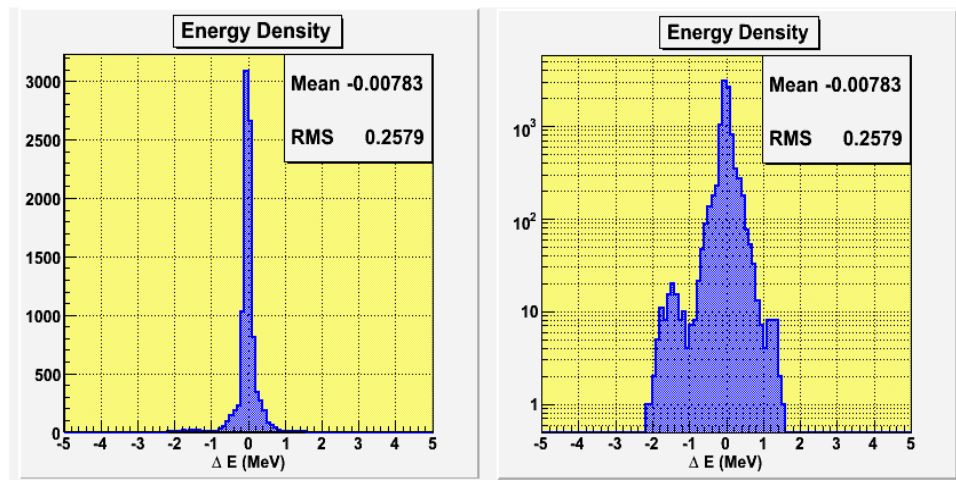


Figure 1.5: Zero-centered energy density; (left) on a linear scale (right) on a logarithmic scale

The principal MI RF is 53 (MHz) and the SC-linac bunching frequency is 325 (MHz). From the MI RF, we can obtain an integer harmonic number of 588. The width of a MI RF bucket is 18.935 (ns), into which trains of microbunches are repeatedly injected over 270 turns, filling in a MI RF bucket in the region of ± 6 (ns) around the center of a MI RF bucket. The beam notch that is kept free of beams is 3.3 (ns) long, following an earlier injection study with a *long bunch* [10]. In the following sections, we will explore and discuss several microbunch-injection scenarios, based upon the RF parameters used in the present MI operation.

Microbunch-Injection Scenarios for the Main Injector

The goals of the modeling of the time-structured multiturn injection into FMI-2 with a SC linac are threefold:

- (1) To find the optimized Fermilab Main Injector RF system with the following aspects:
 - (i) Efficient RF capture methods with minimum particle losses
 - (ii) Main Injector RF system with adequate RF parameters
 - (iii) Minimization of space-charge effects in all degrees of freedom
 - (iv) Optimization of total capture time and total injection time
- (2) To design a fast beam-chopper system to make nearly loss-free injection attainable
- (3) To investigate any other limitations on the intensity upgrades from the present Main Injector

With the above goals in mind, we modeled four different scenarios of synchronous injection over 270 injection turns, but with different RF harmonic systems and RF parameters. The following is the parameters of the Main Injector that are consistently employed in ESME simulations for all scenarios presented herein.

Table 1.1: Main Injector Parameters for ESME Simulations

Mean Radius	528.297 (m)
Beam Momentum (at injection)	8.889 (<i>GeV/c</i>)
γ_{tr}^2 (transition gamma)	466.53572
Principal Harmonic No.	588
Φ_s (synchronous phase)	0.0 (deg)
effective beam radius (at injection)	0.0050 (m)
effective beam-pipe radius (at injection)	0.051 (m)
No. of Space-Charge Bins	64
No. of FFT Bins	64
Microbunch Intensity	2.65×10^8
Total Intensity (after injection is complete)	1.54×10^{14}

SCENARIO (I)

- synchronous injection of a train of 4 microbunches into a standing RF bucket
- single RF Harmonic (53 MHz)
- $V_{rf} = 800$ (kV) (fixed RF voltage with no ramping)
- 270 **injection turns** (~ 3 ms) \rightarrow 2,700 turns (~ 30 ms)
- longitudinal space charge included
- longitudinal painting in RF-phase (θ) direction

We begin with a single RF system of 53 (MHz) and the fixed RF voltage (V_{rf}) of 800 (kV). Referring to Figure 1.3, a series of four blobs captured in a RF bucket represent the first train of microbunches that are synchronously injected into a standing RF bucket. The dotted sinusoidal curve for RF voltage waveform in the background of the phase-space figure indicates the single RF harmonic and the amplitude of RF voltage.

The single turn in the MI in terms of the average machine circumference and the revolution period can be expressed as follows:

$$360 \text{ (deg)} = 11.1338 \text{ (\mu s)} = 3319.388 \text{ (m)} \quad (1.2)$$

For one MI RF bucket, the following Eqn. (1.3) is obtained from Eqn. (1.2) as illustrated in Figure 1.2.

$$52.8114 \text{ (MHz)} = 18.9353 \text{ (ns)} = 0.6122 \text{ (deg)} = 5.645 \text{ (m)} \quad (1.3)$$

Due to the *longitudinal mismatch*, or *RF mismatch* between the SC linac and the FMI-2, an inherent phase slip between 325-MHz microbunch structure and the MI stationary buckets could be parasitically induced in the form of longitudinal painting in RF-phase direction. With f and λ being radio frequency and RF wavelength, respectively, we computed the RF ratio (\mathcal{R}_{rf}).

$$\begin{aligned} \mathcal{R}_{\text{rf}} &= \frac{f_{PD}}{f_{MI}} = \frac{325 \text{ MHz}}{52.8114 \text{ MHz}} \\ &= \frac{\lambda_{MI}}{\lambda_{PD}} = \frac{5.6453 \text{ (m)}}{0.9173 \text{ (m)}} \\ &= 6.154 \end{aligned} \quad (1.4)$$

Referring to Figure 1.2, Eqn. (1.4) implies that a total of 6 linac RF buckets of 325 MHz can fit in one MI RF bucket. Since the RF ratio is a non-integer number, a modulus of the RF ratio is computed as for the case of the Booster injection modeling [1].

$$\mathcal{R}_{\text{rf}} \Big|_{\text{mod}} = 0.154 \quad (1.5)$$

One can then arrive at the range of phase slip within one MI RF bucket.

$$0.155 \times 0.0995 \text{ (deg)} = 0.0154 \text{ (deg)} \quad (1.6)$$

Figure 1.6 shows trains of microbunches and *discrete* charge distribution after 3 injection turns with phase slips included. For each successive MI RF bucket, the 325-MHz bunches advance by 0.0154 (deg). Hence, it is estimated that every 6 turns the phase of injected microbunches slips through one 325-MHz bucket.

$$\delta\theta_{rf} = \frac{0.0995 \text{ (deg)}}{0.0154 \text{ (deg)}} = 6.46 \quad (1.7)$$

Having this amount of phase slip included, we simulated the SC linac-to-MI injection with ESME over 270 injection turns. After the 270 turns, the longitudinal phase space is painted in RF-phase space as illustrated by Figure 1.7. As in Figure 1.8, one-peaked but *continuous* distribution of charge density⁶ at the 270-th turn is shown. The evolution of longitudinal emittance growth for the case of a single RF harmonic is shown in Figure 1.9. As the number of macroparticles increases, so does the longitudinal emittance up to about 0.08 (eV-s). Then, the emittance flattens out until the end of the simulation run. The induced voltage (\mathcal{V}_{sc}) due to space-charge fields ($\mathcal{E}(z)$) is proportional to the *g-factor*, which is usually defined as $1 + 2\ln(R_w/R_b)$. Hence, from the charge distribution, space-charge-induced voltage per turn is computed at a specified turn. In particular, we looked at the induced voltage at the last injection turn of 270-th turn as shown in Figure 1.11.

$$\mathcal{V}_{sc} \propto \frac{1}{\beta\gamma^2} \cdot \left[1 + 2\ln(R_w/R_b) \right] \quad (1.8)$$

where R_w , and R_b denote effective beam pipe radius, and effective beam radius, respectively. In the case of the Main Injector at injection energy of 8.0 GeV, the *g-factor* is about 5.64. In Figure 1.12, the peak collective voltage in frequency domain (\hat{V}_{FD}) is drawn at each turn. The collective voltage goes up to about 50.0 (keV) at the end of the injection.

⁶Charge density, or *azimuthal density* is referred to as charge line density, for convenience.

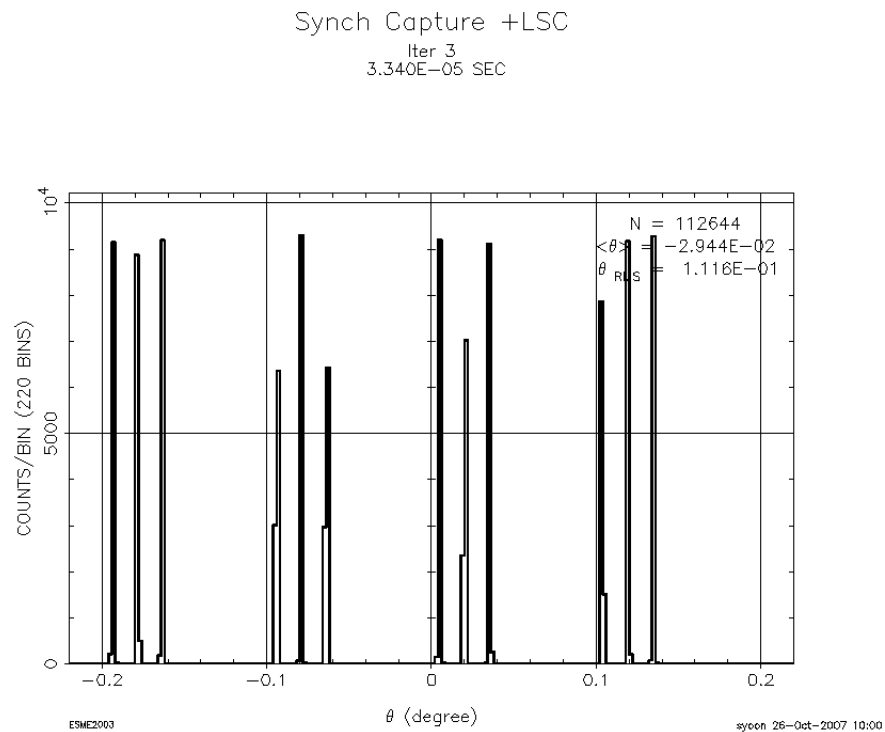
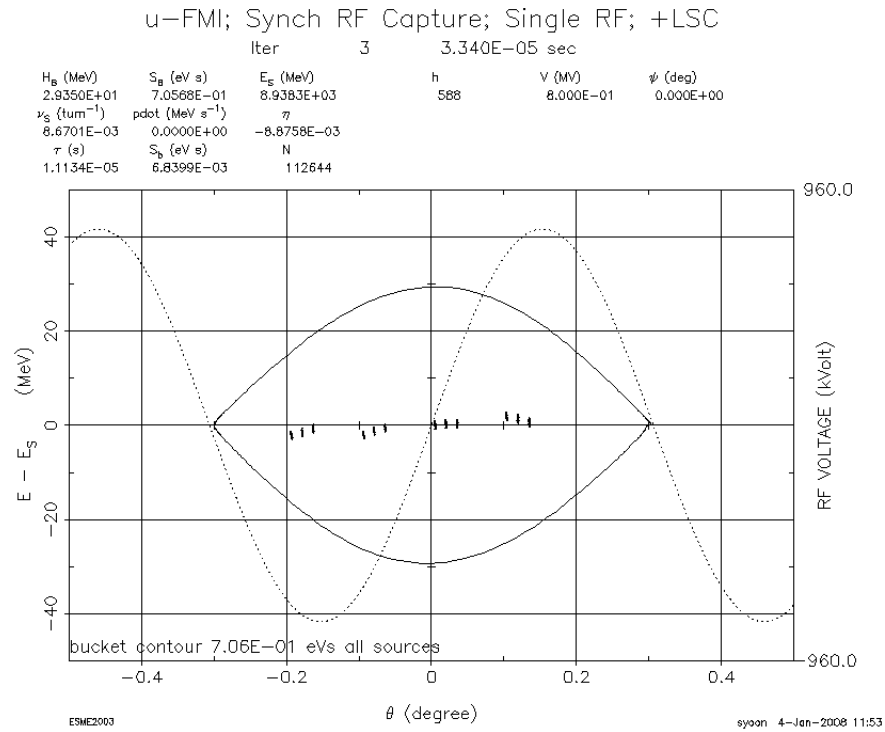
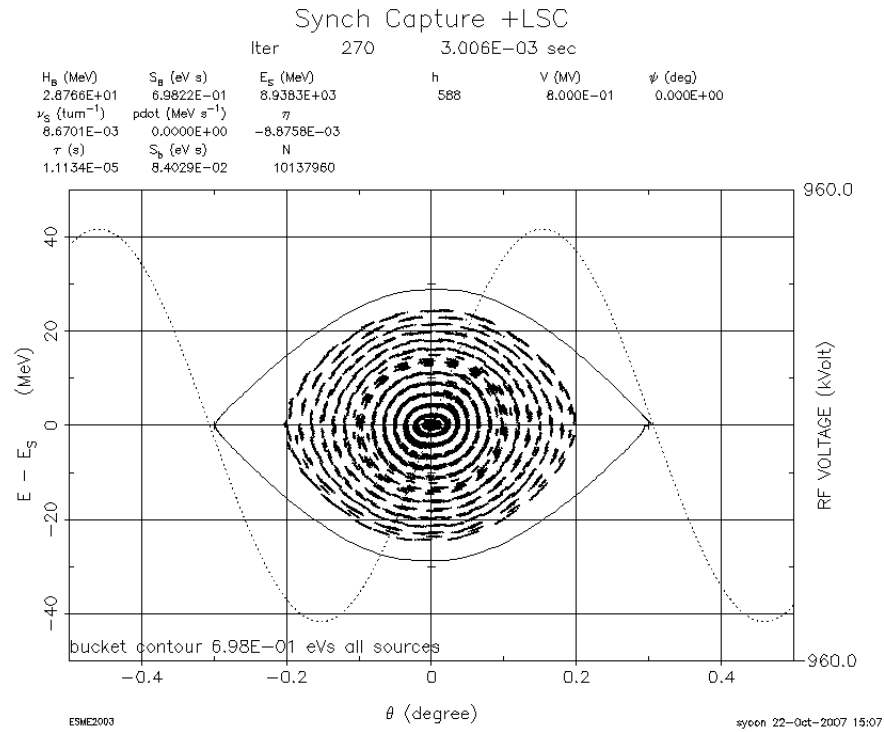
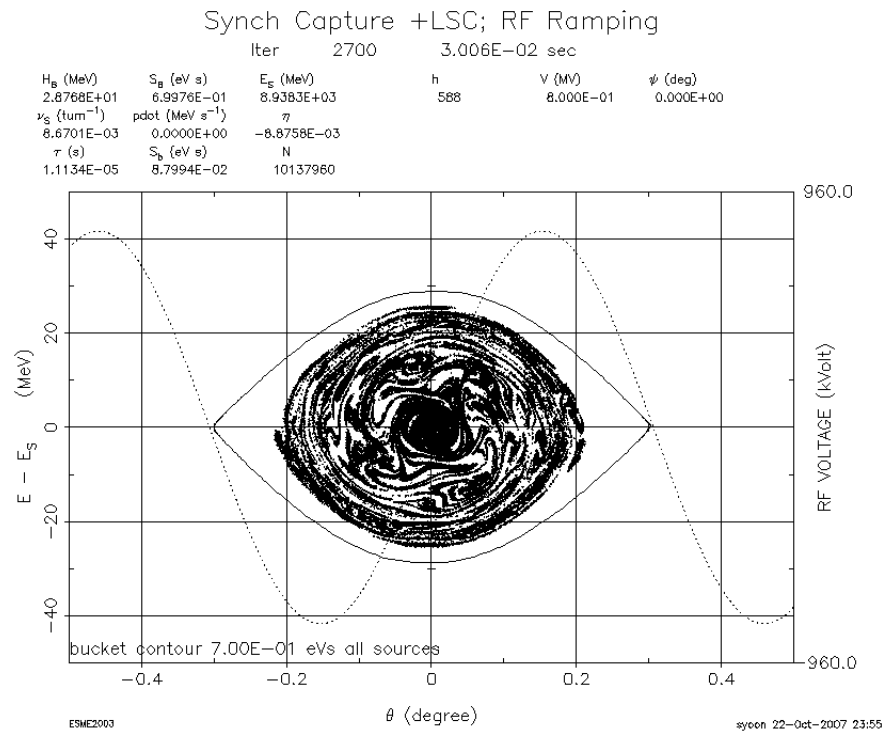


Figure 1.6: [Scenario (I)] Phase space and discrete charge density after 3 injection turns



(a) 270 turns

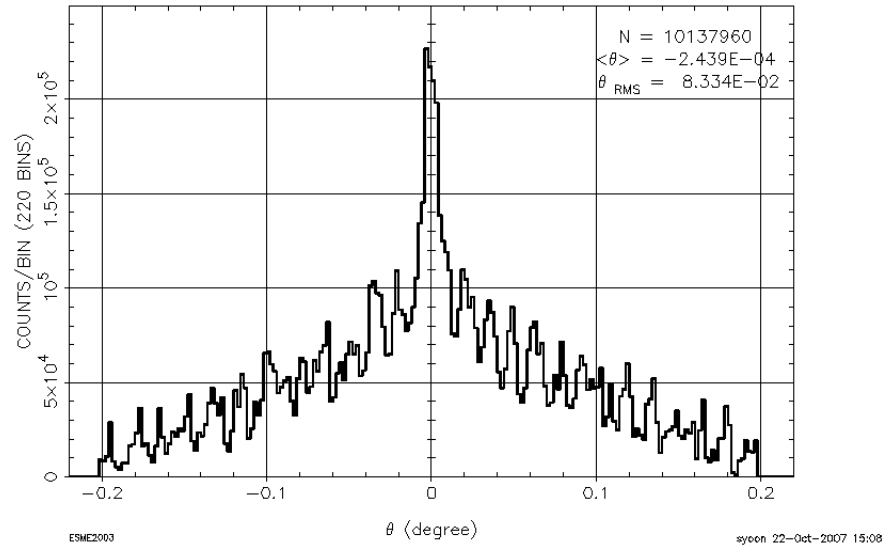


(b) 2,700 turns

Figure 1.7: [Scenario (I)] Synchronous injection of microbunches with a single RF system (a) after 270 turns (b) after 2,700 turns; Note that LSC in the figure title stands for Longitudinal Space Charge.

Synch Capture +LSC

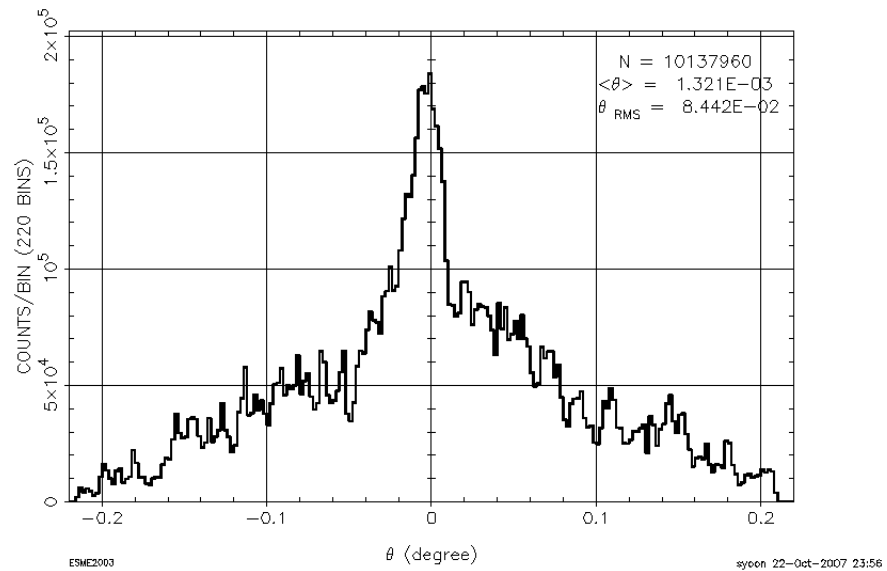
Iter 270
3.006E-03 SEC



(a) 270 turns

Synch Capture +LSC; RF Ramping

Iter 2700
3.006E-02 SEC



(b) 2,700 turns

Figure 1.8: [Scenario (I)] Distribution of charge density with single RF harmonic at the 270-th turn and at the 2,700-th turn.

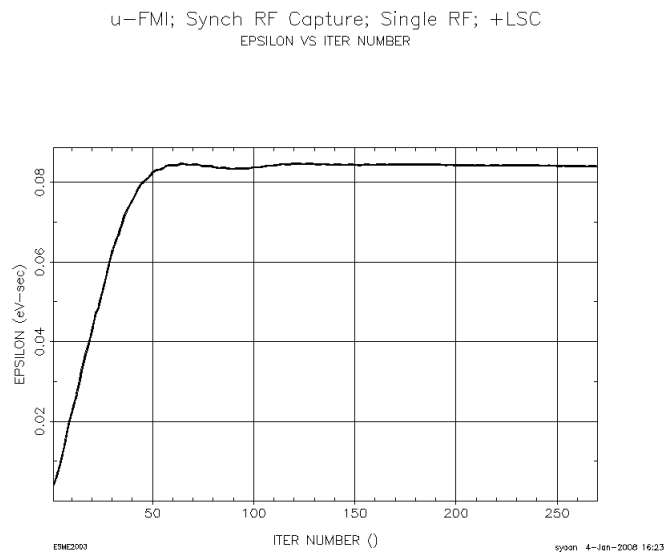


Figure 1.9: [Scenario (I)] Evolution of longitudinal emittance with a single RF harmonic over 270 turns

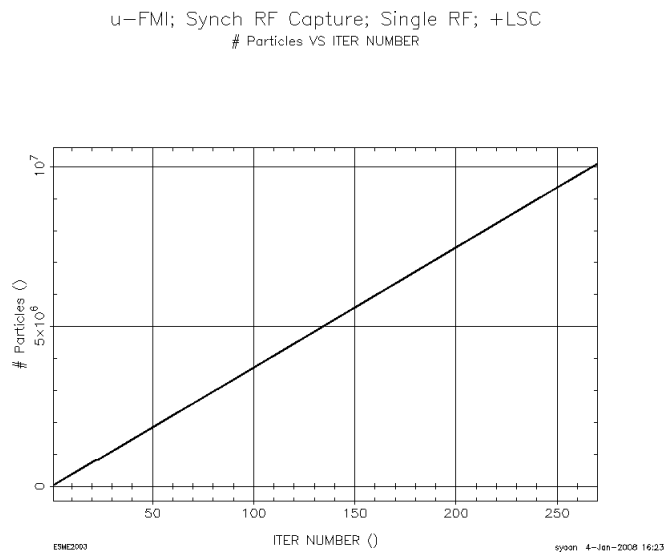


Figure 1.10: [Scenario (I)] Evolution of the number of injected macroparticles with a single RF harmonic over 270 turns

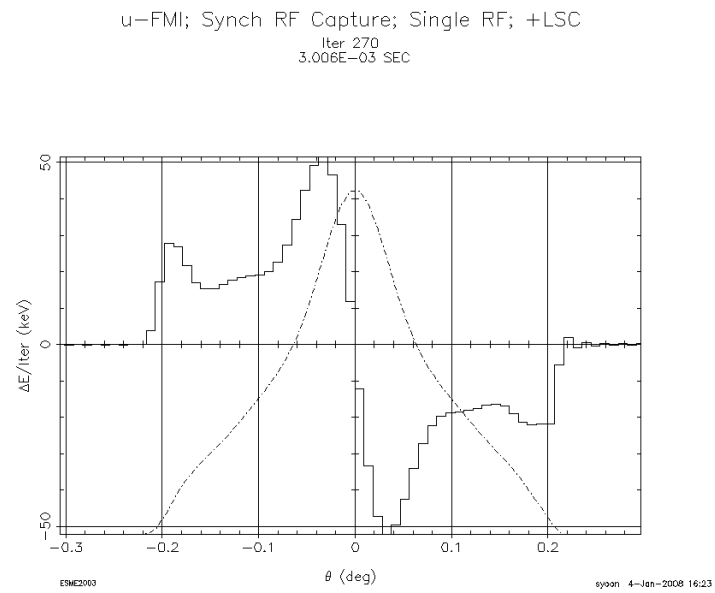


Figure 1.11: [Scenario (I)] Induced ΔE per turn due to space charge ($\Delta E/\text{turn}$) with a single RF harmonic at 270^{th} turn

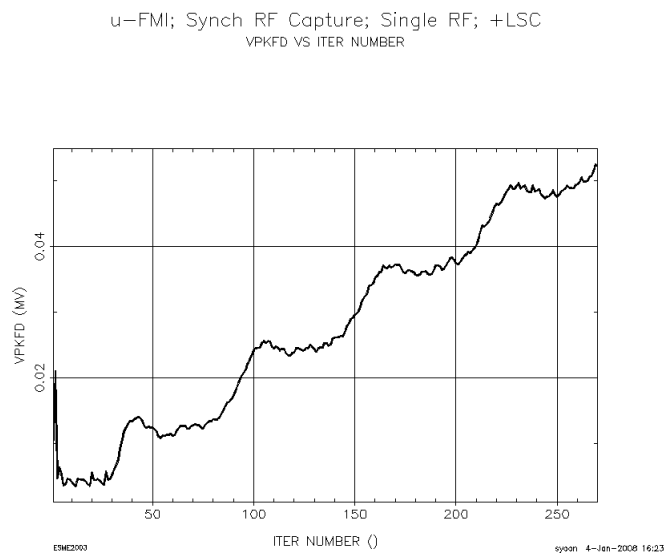


Figure 1.12: [Scenario (I)] Time evolution of collective voltage in frequency domain over 270 turns

u-FMI; Synch RF Capture; Single RF; +LSC
Bunching Factor VS ITER NUMBER

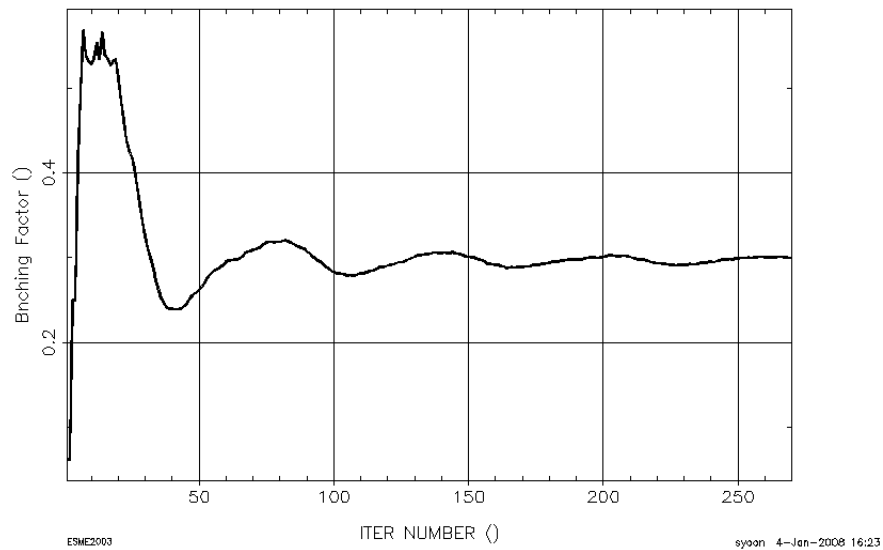


Figure 1.13: [Scenario (I)] Time evolution of bunching factor

As the bunching factor is usually defined as average current ($\langle I \rangle$) over peak current (\hat{I}) for convenience, the value is upper-bounded at unity. Figure 1.13 shows that the bunching factor converges to about 0.3 for the case of Scenario (I).

SCENARIO (II)

In Scenario (II), the injection process described in Scenario (I) is followed by ramping up the RF voltage linearly up to 150 % of the initial RF voltage. Thus, the RF voltage ramping lasts for additional 27 (ms), and the total injection time elapses about 30 (ms).

- $V_{rf, i} = 800$ (kV), $V_{rf, f} = 1,200$ (kV)
- ramping RF voltage after the injection is complete

At the end of RF voltage ramping, the macroparticles are well captured in a RF bucket as shown in Figure 1.14. Figure 1.15 shows the variation of RF voltage from 800 (kV) to 1,200 (kV) starting from the 270-th turn through the 2,700-th turn. In comparison to Figure 1.8 from Scenario (I), the gradient of charge distribution ($d\lambda/dz$) are reduced and spread more out with ramping RF voltage over extended 2,700 turns (cf. Figure 1.16). However, it still shows a peaked distribution centered around the origin. The longitudinal emittance (ϵ_l) grows up to 0.085 (eV-s) with a fixed RF voltage at 800. (kV). Once the RF voltage starts ramping linearly, the emittance continues to grow gradually up to 0.09 (eV-s) as shown in Figure 1.17.

In an attempt to reduce further the space-charge-induced voltage and to produce a more uniform charge distribution, a dual RF harmonic system is explored in Scenarios (III) and (IV) in the following subsections.

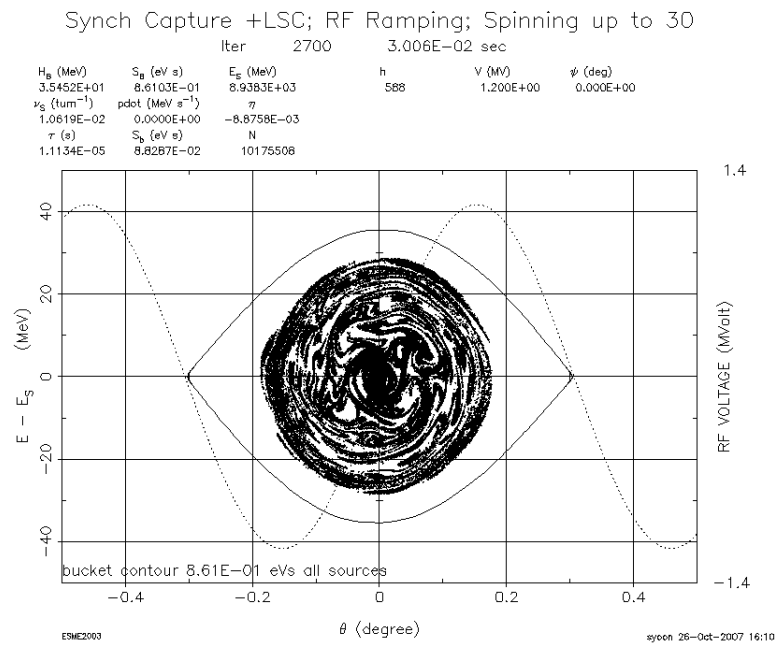


Figure 1.14: [Scenario (II)] Synchronous injection of microbunches with a single RF harmonic and ramping RF voltage

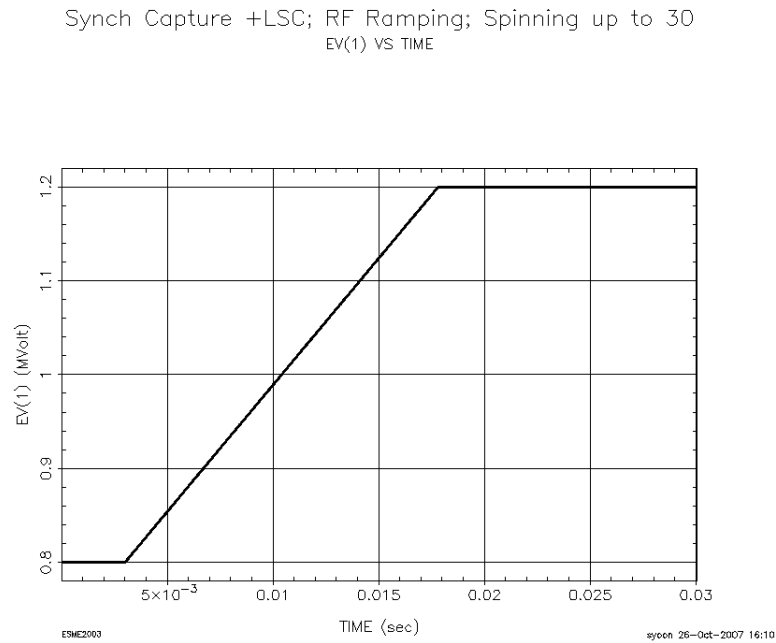


Figure 1.15: [Scenario (II)] RF voltage curve over 2,700 turns

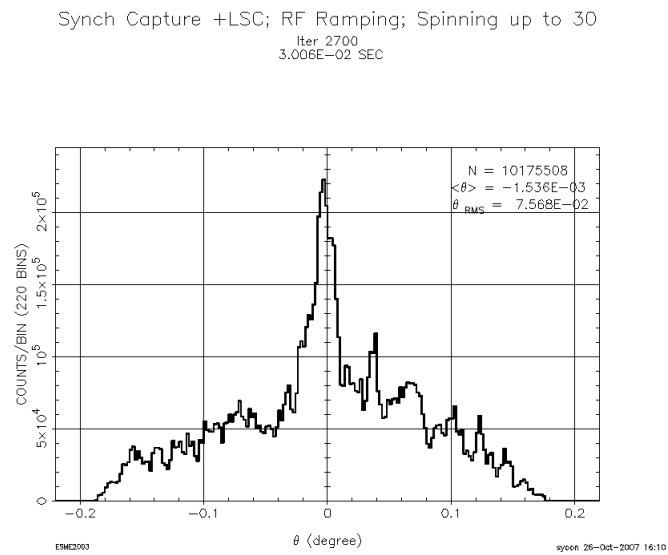


Figure 1.16: [Scenario (II)] Distribution of charge density with a single RF harmonic and ramping RF voltage after 2,700 turns

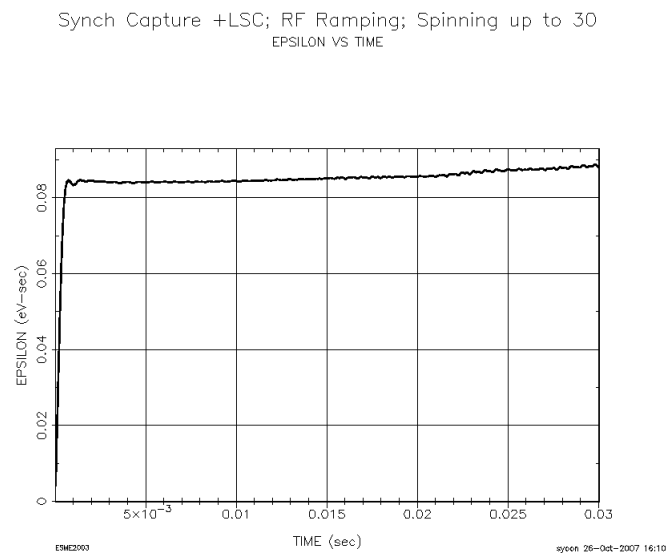


Figure 1.17: [Scenario (II)] Time evolution of longitudinal emittance (ϵ_l) with a single RF system

SCENARIO (III)

- Dual RF Harmonics:

$$f_{rf, 1} = 53 \text{ MHz and } f_{rf, 2} = 106 \text{ MHz}$$

- $H_1 = 588$ and $H_2 = 1176$

$$R_H = H_2/H_1 = 2.0$$

- $V_{rf, 1} = 400. \text{ (kV)}$ and $V_{rf, 2} = 300. \text{ (kV)}$ (fixed RF voltages)

$$R_H = V_{rf, 2}/V_{rf, 1} = 0.75$$

In scenario (III), a dual RF harmonic system of 400 (kV) on 53 (MHz) and 300 (kV) on 106 (MHz) is explored. The higher-order RF harmonic ($H_2 = 1176$) is twice of the principal RF harmonic ($H_1 = 588$). The secondary RF voltage ($V_{rf, 2}$) is 75 % of the principal RF voltage ($V_{rf, 1}$). The RF voltage waveform of the higher harmonic for a dual RF system can be

$$\mathcal{V} = \mathcal{V}'_{rf, 1} \sin(H_1\phi_1 + \psi_1) + \mathcal{V}'_{rf, 2} \sin(H_2\phi_2 + \psi_2), \quad (1.9)$$

where \mathcal{V}'_{rf} , H , ϕ , and ψ are RF voltage, harmonic number, phase angle of each macroparticle, and phase of RF cavity, respectively. As can be seen in Figure 1.18, the waveform has a negative slope around the stable phase of 0 (deg). By adding a higher secondary harmonic RF voltage to a principal harmonic RF voltage, we can create a flat-bottom potential energy. As a result, the RF-bucket contour with a dual RF system is also flattened at the top and bottom on a phase-space plot. Hence, the charge distribution follows the flat contour shape. Also, the principal RF voltage can be half as high as the RF voltage used for the case of single RF harmonic. Since the flat-bottom potential energy irons out the peaked charge distribution, the utilization of a dual RF system gives a great advantage to the single RF system. Eventually, the dual RF system will help us lower the beam-current limitations caused by space-charge effects. After 2,700 turns, the formation of localized macroparticle

distributions are observed around three local bumps of the dual-harmonic voltage waveform. Figure 1.20 shows the time evolution of injected macroparticles inside a dual RF bucket. From turn 1 through turn 270, a train of four microbunches are injected with parasitic phase offsets. After the injection process is complete, in order to reach an equilibrium state, injected macroparticles are circulated up to 2,700 turns with no further injection. Note that as time elapses after the completion of injection process, sporadic white gaps in between lumps of macroparticles are gradually disappeared. In Figures from 1.22 through 1.24 three plots of longitudinal phase space, charge density, and energy density comprise each row corresponding to turn number under a phase-space plot. With the choice of RF voltages $R_V = 0.75$, a bi-modal charge distribution is created due to a pair of potential wells around the stable phase of 0 (deg). However, with the help of longitudinal painting, the contour of charge distribution becomes smoother as the turn number increases, but the dual peaks remain in the charge distribution.

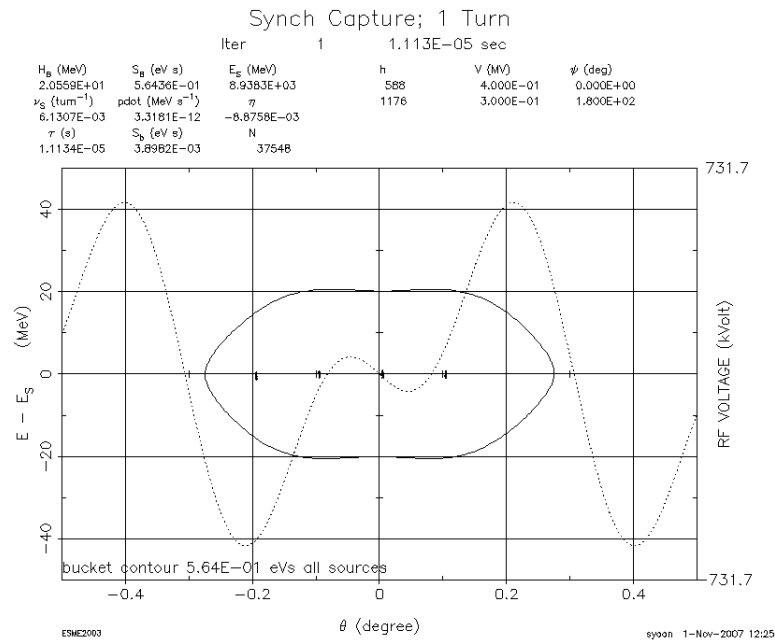


Figure 1.18: [Scenario (III)] RF bucket and dual RF waveform in the background

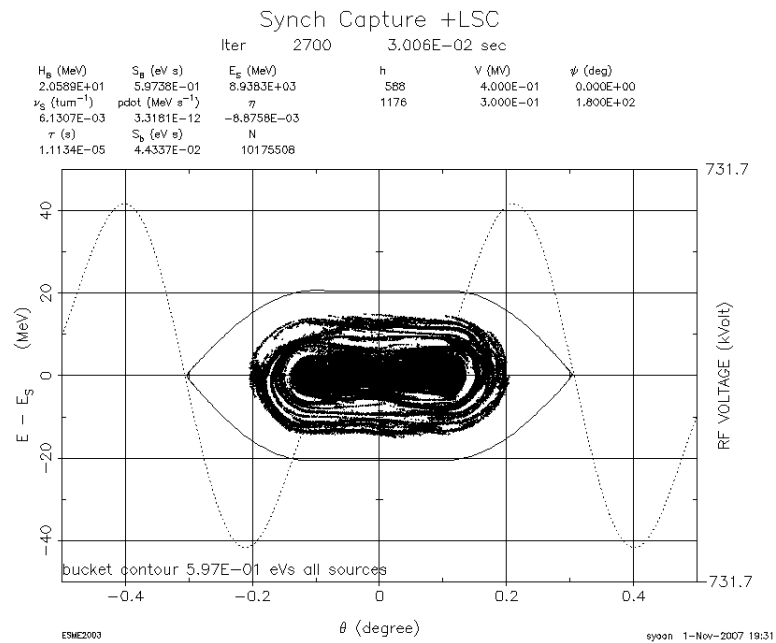
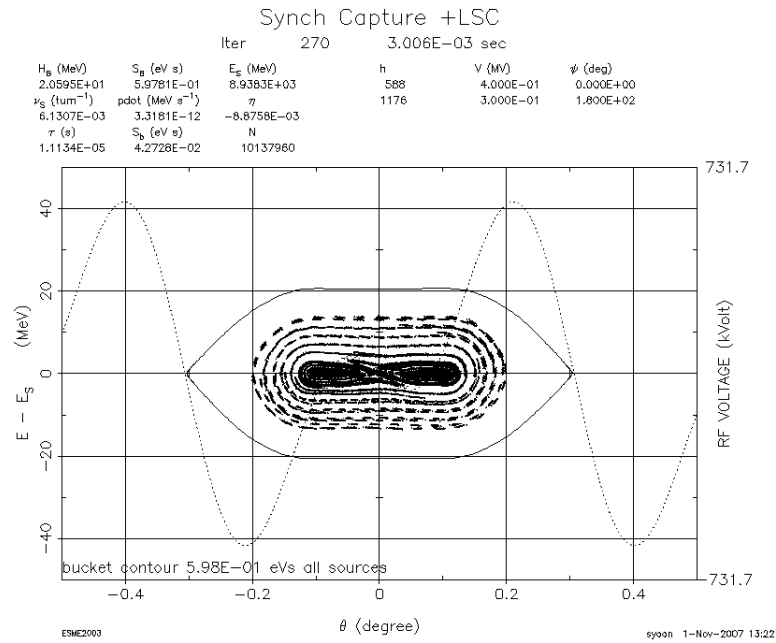
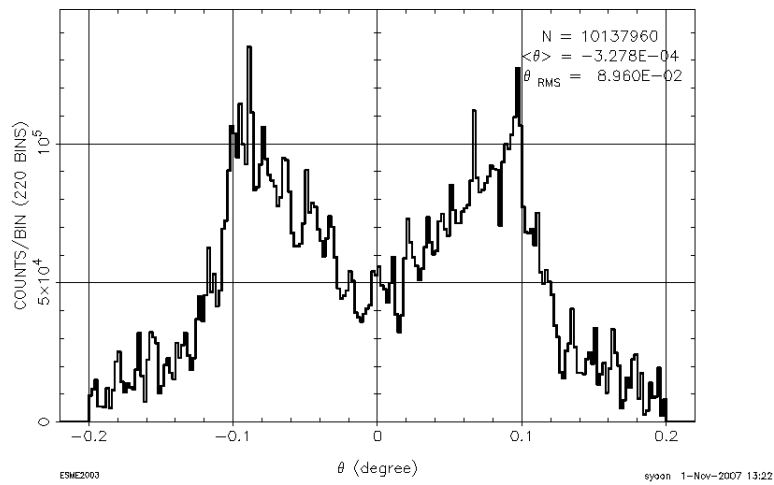


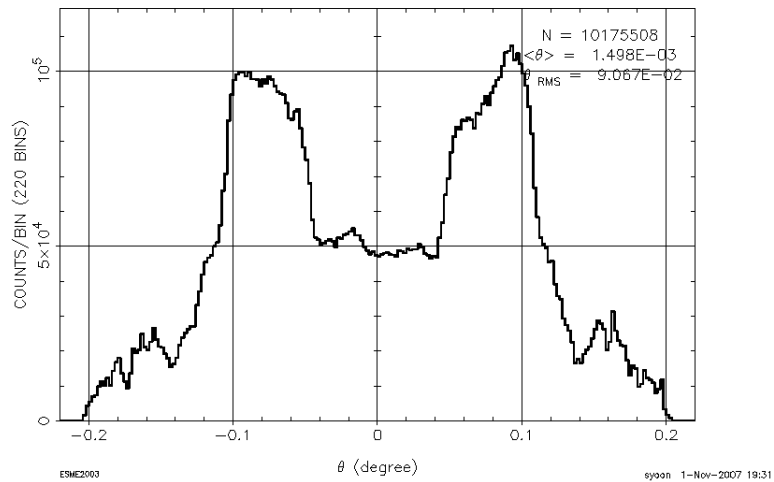
Figure 1.19: [Scenario (III)] Distribution of macroparticles with longitudinal painting

Synch Capture +LSC

Iter 270
3.006E-03 SEC

(a) after 270 turns

Synch Capture +LSC

Iter 2700
3.006E-02 SEC

(b) after 2,700 turns

Figure 1.20: [Scenario (II)] Distribution of charge density with longitudinal painting included

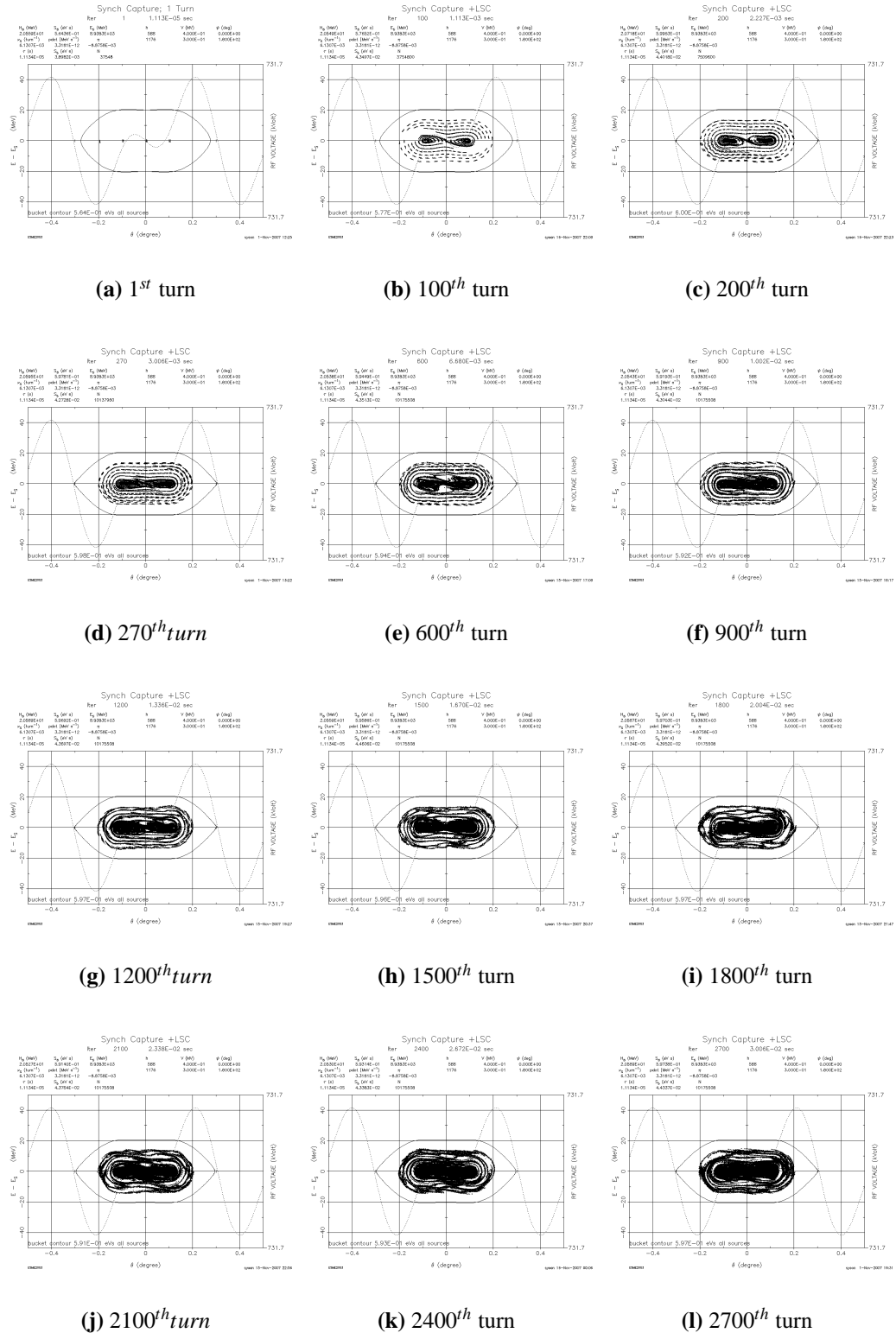


Figure 1.21: [Scenario (III)] Time evolution of phase space with longitudinal painting included, starting from the 1st injection turn through 2700 turns

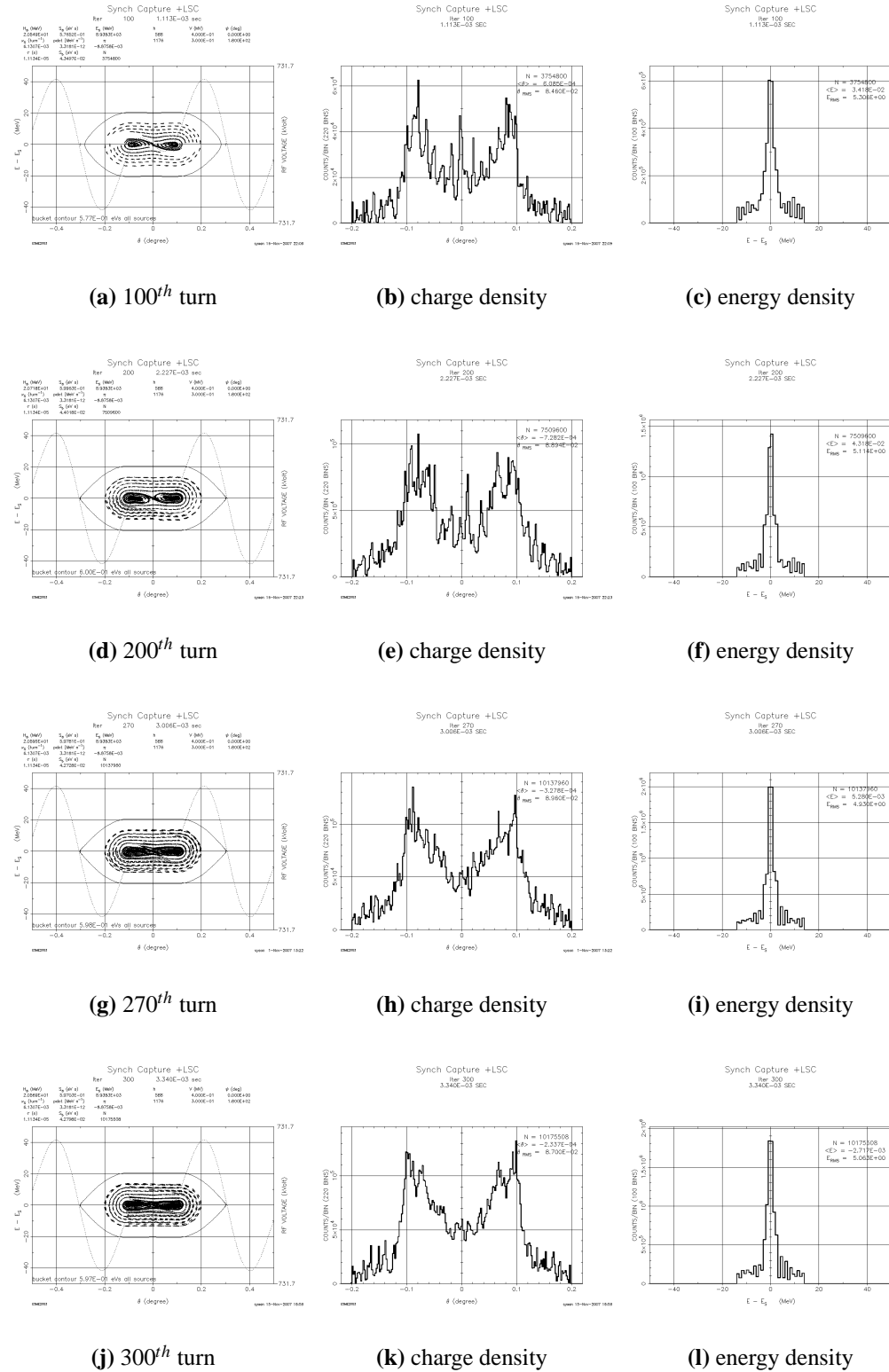


Figure 1.22: [Scenario (III)] Time evolution of phase space with longitudinal painting starting from 100th turn through 300th turns

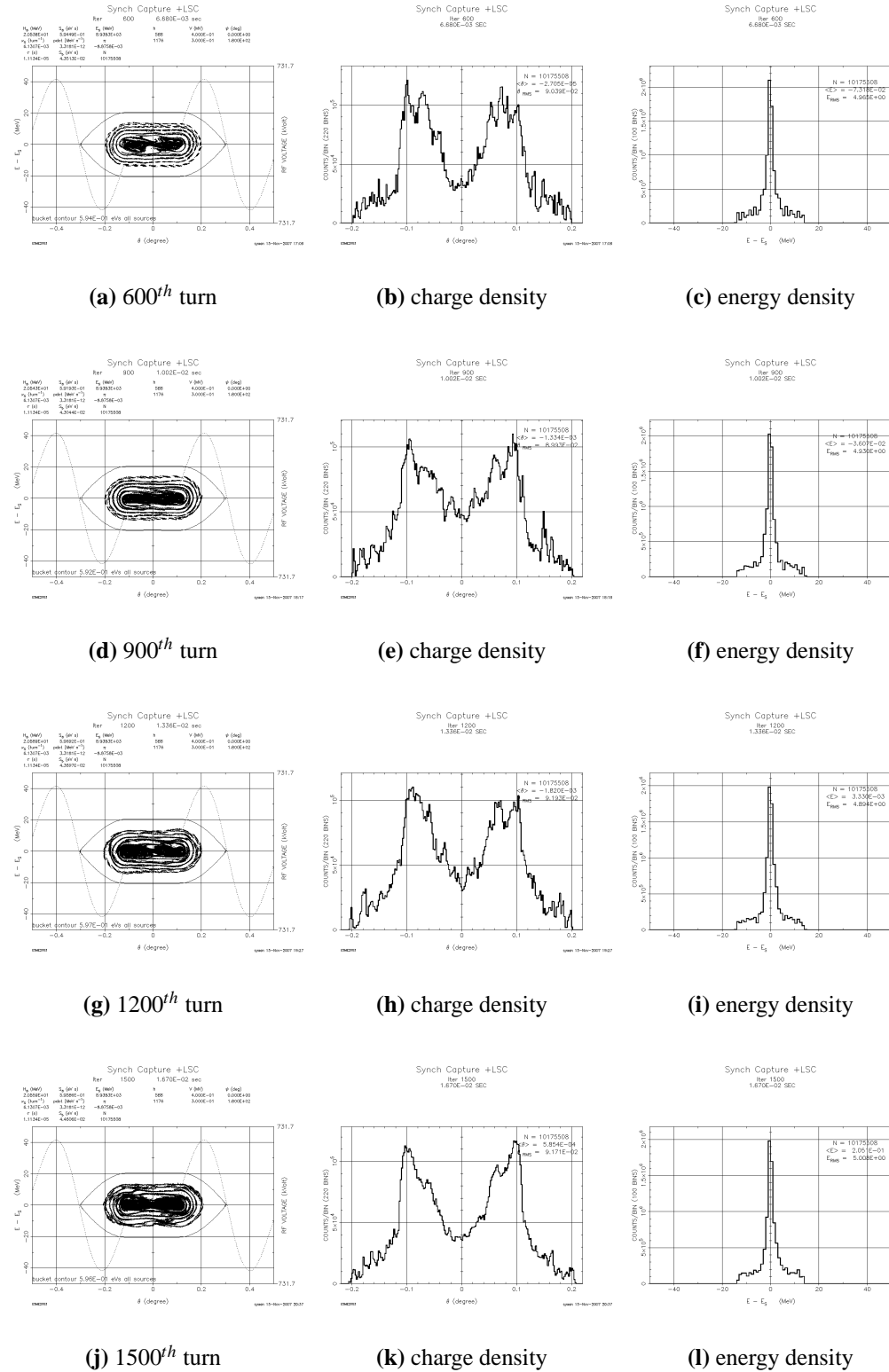


Figure 1.23: [Scenario (III)] Time evolution of phase space with longitudinal painting starting from 600th turn through 1500th turns

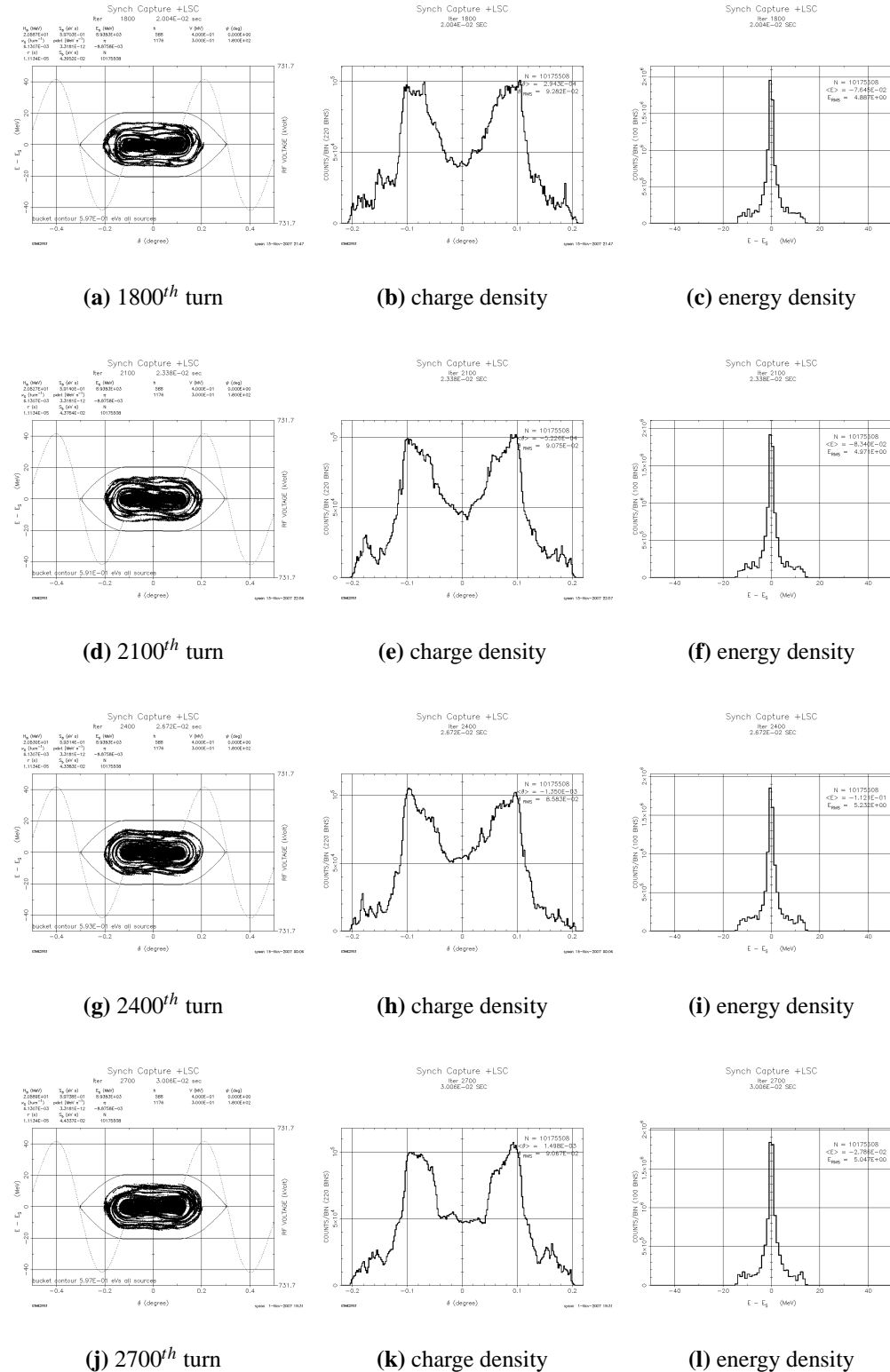


Figure 1.24: [Scenario (III)] Time evolution of phase space with longitudinal painting starting from 1800th turn through 2700th turns

SCENARIO (IV)

- Dual RF Harmonics:

$$f_{rf, 1} = 53 \text{ MHz} \text{ and } f_{rf, 2} = 106 \text{ MHz}$$

$$H_2 = 1176 \text{ and } H_1 = 588$$

$$R_H = f_{rf, 2} / f_{rf, 1} = 2.0$$

- $V_{rf, 1} = 400 \text{ (kV)}$ and $V_{rf, 2} = 200 \text{ (kV)}$ (fixed RF voltages)

Scenario (IV) is under the same conditions as in scenario (III), except that the secondary RF voltage is 50 % of the principal RF voltage. It is more advantageous in that the RF waveform has a nice plateau around the stable phase of 0 (deg) as shown in Figure 1.25. Through the longitudinal painting at each turn, a total of 1080 (270×4) microbunches that are injected over 270 turns and further circulated up to 30 (ms) gradually transform into a continuous *macrobunch*, or *long bunch* spanning in between -0.2 (deg) and +0.2 (deg). Unlike in Figure 1.20 (a), localization of macroparticles is not observed in Figure 1.27 (a) after the injection of 270 turns is complete. After further circulation of beams up to 2,700 turns with no further injection, the beam charge distribution becomes smoother in the region of -0.2 (deg) and +0.2 (deg). (see Figures 1.19 and 1.20). As a consequence, the bi-modal distribution of charge density observed from the outcome of Scenario (III) is not observed as shown in Figures 1.22 through 1.24. As the number of injected macroparticles increases, longitudinal painting progresses, and time elapses, the fine structure of charge distribution gradually disappears. Eventually, after the 2,700 turns, the contour of charge distribution becomes smoother. Including phase offsets without energy jitter, this effect stands out in charge distribution, rather than energy distribution as observed in Scenario (III).

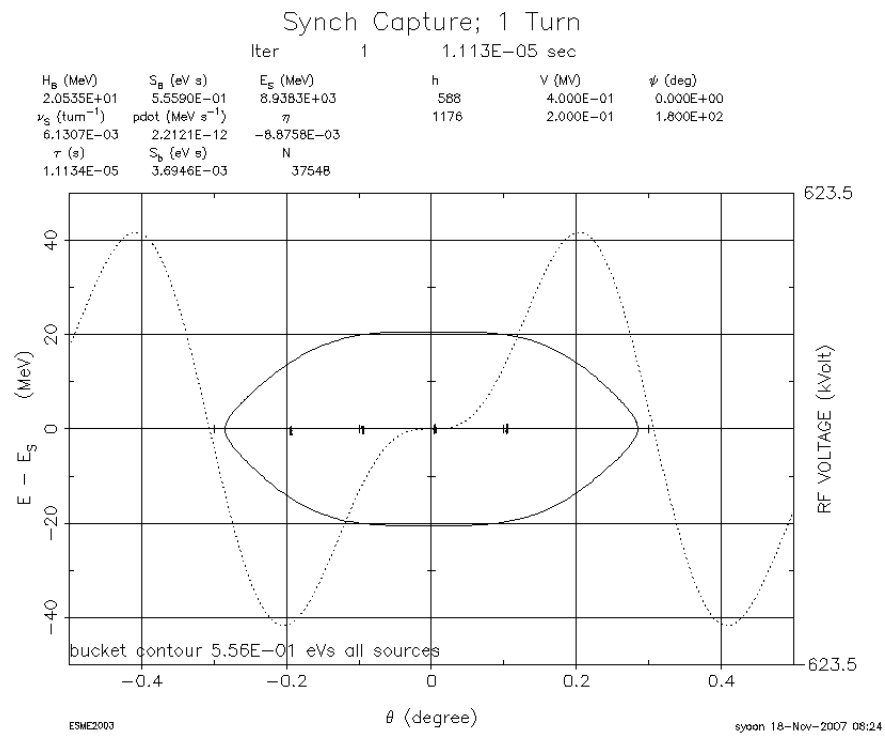
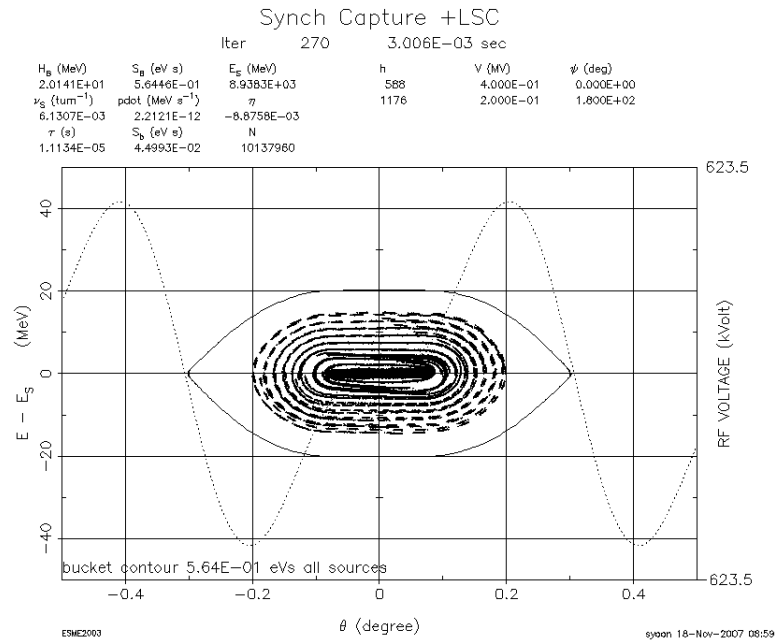
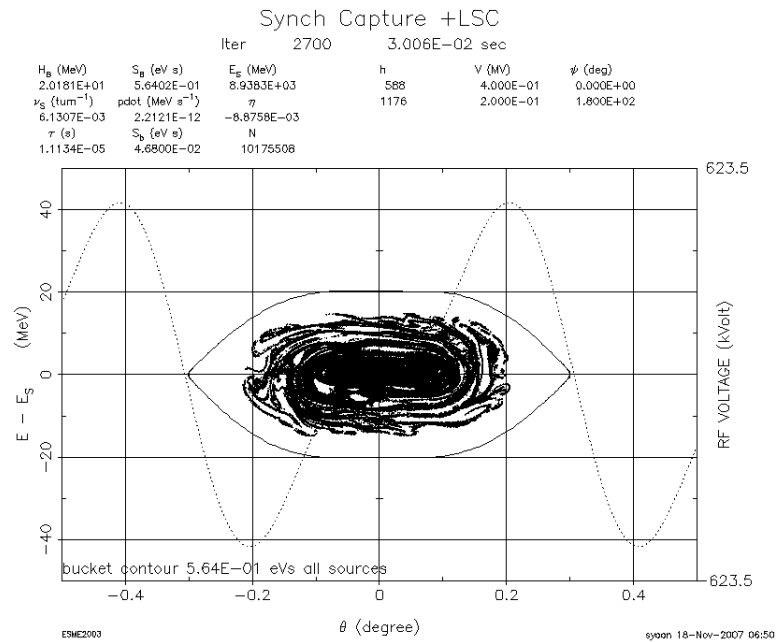


Figure 1.25: [Scenario (IV)] RF waveform for a dual RF system with the RF voltage ratio of 0.5



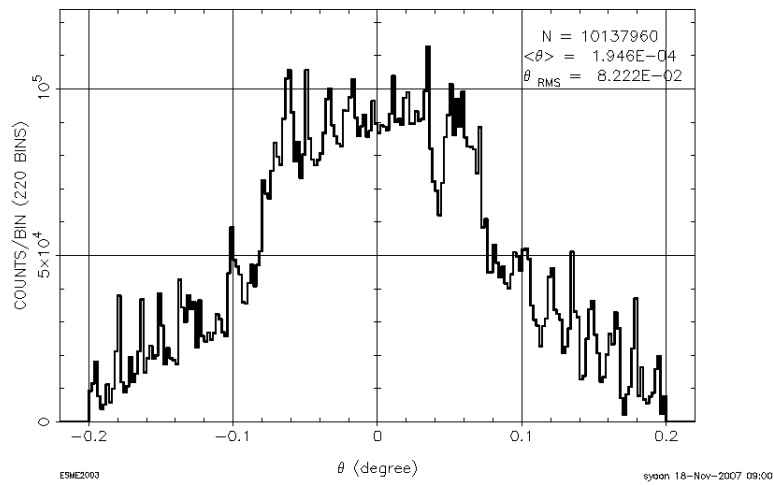
(a) at the 270-th turn



(b) at the 2,700-th turn

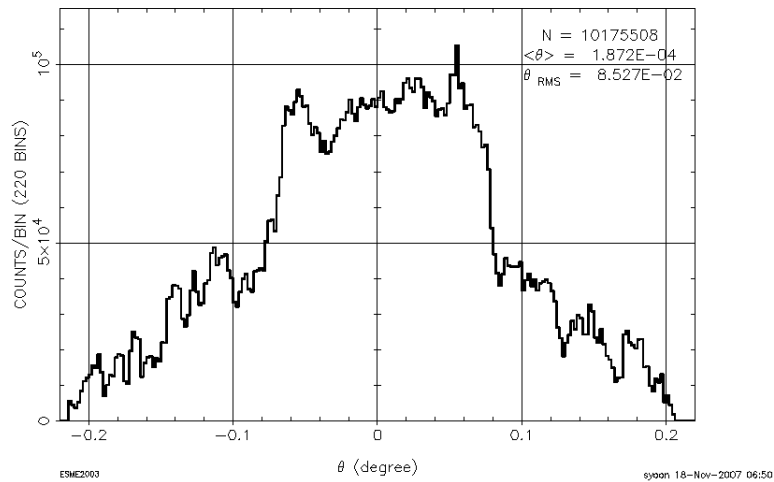
Figure 1.26: [Scenario (IV)] Synchronous injection of microbunches with a dual RF harmonic (a) at 270th turns and (b) at 2700th turns

Synch Capture +LSC

Iter 270
3.006E-03 SEC

(a) at the 270-th turn

Synch Capture +LSC

Iter 2700
3.006E-02 SEC

(b) at the 2,700-th turn

Figure 1.27: [Scenario (IV)] Distribution of charge density with a dual RF harmonic (a) at 270^{th} turns and (b) at 2700^{th} turns

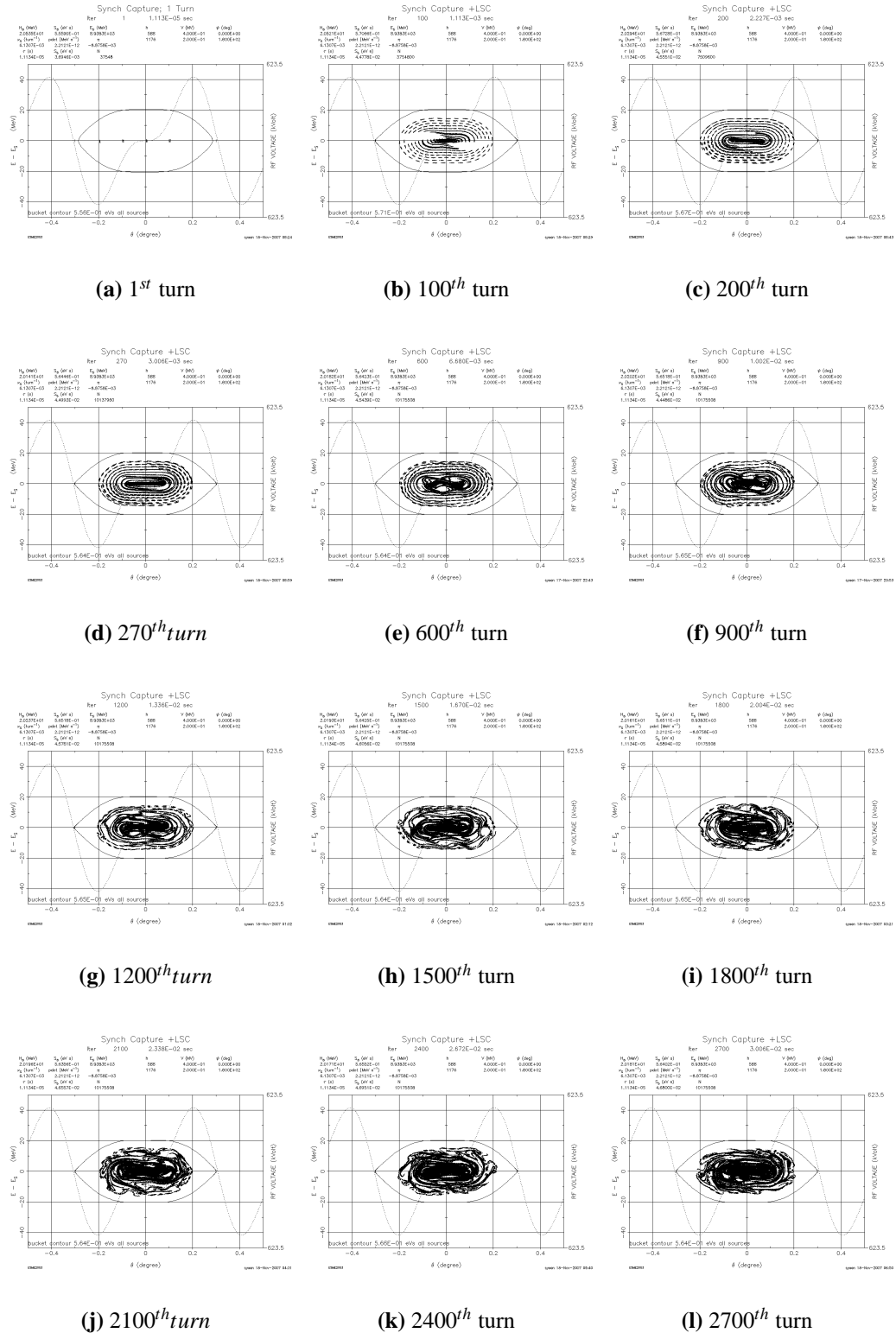


Figure 1.28: [Scenario (IV)] Time evolution of phase space with longitudinal painting included, starting from the 1st injection turn through 2700 turns

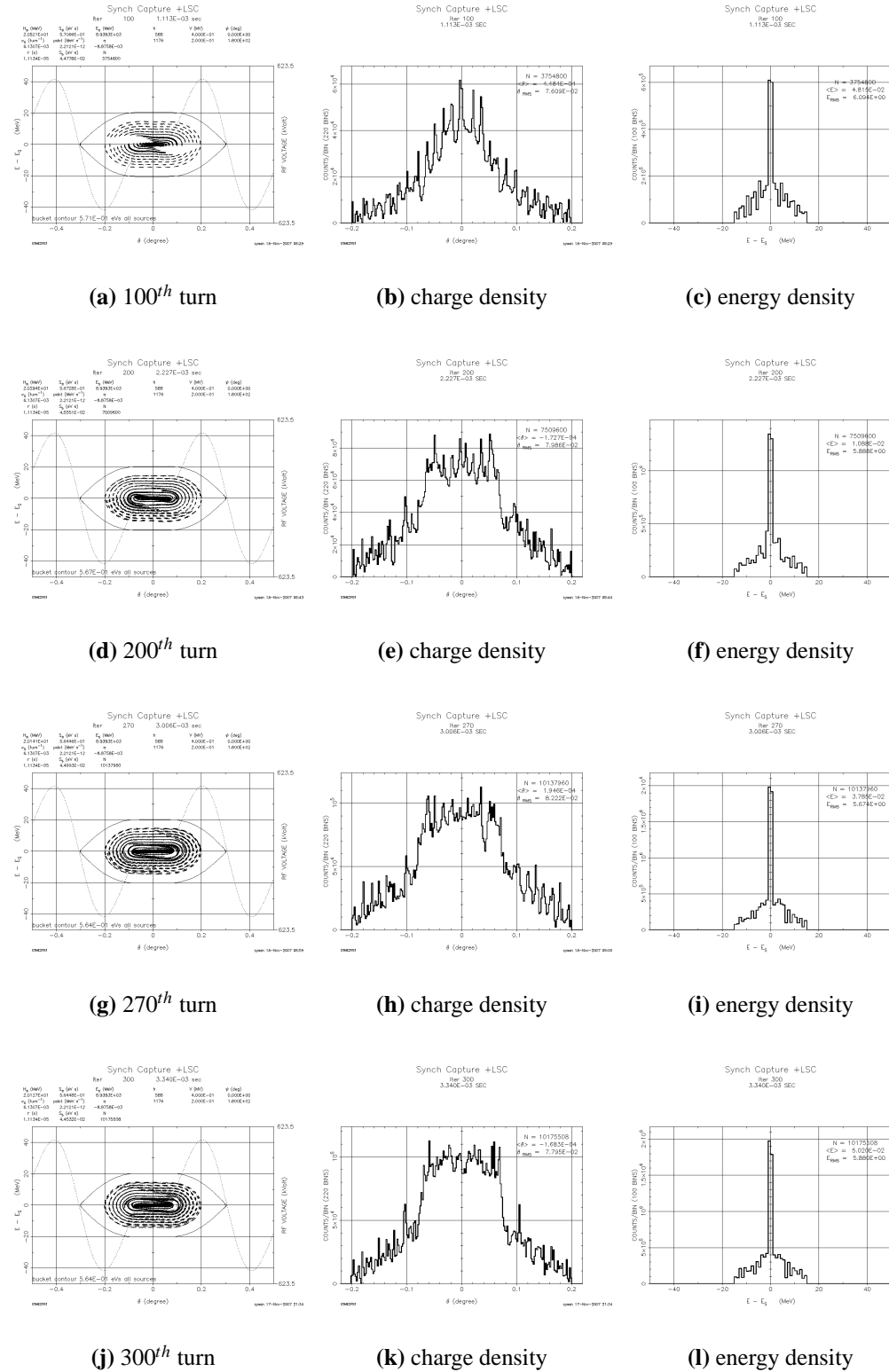


Figure 1.29: [Scenario (IV)] Time evolution of phase space with longitudinal painting starting from 100th turn through 300th turns

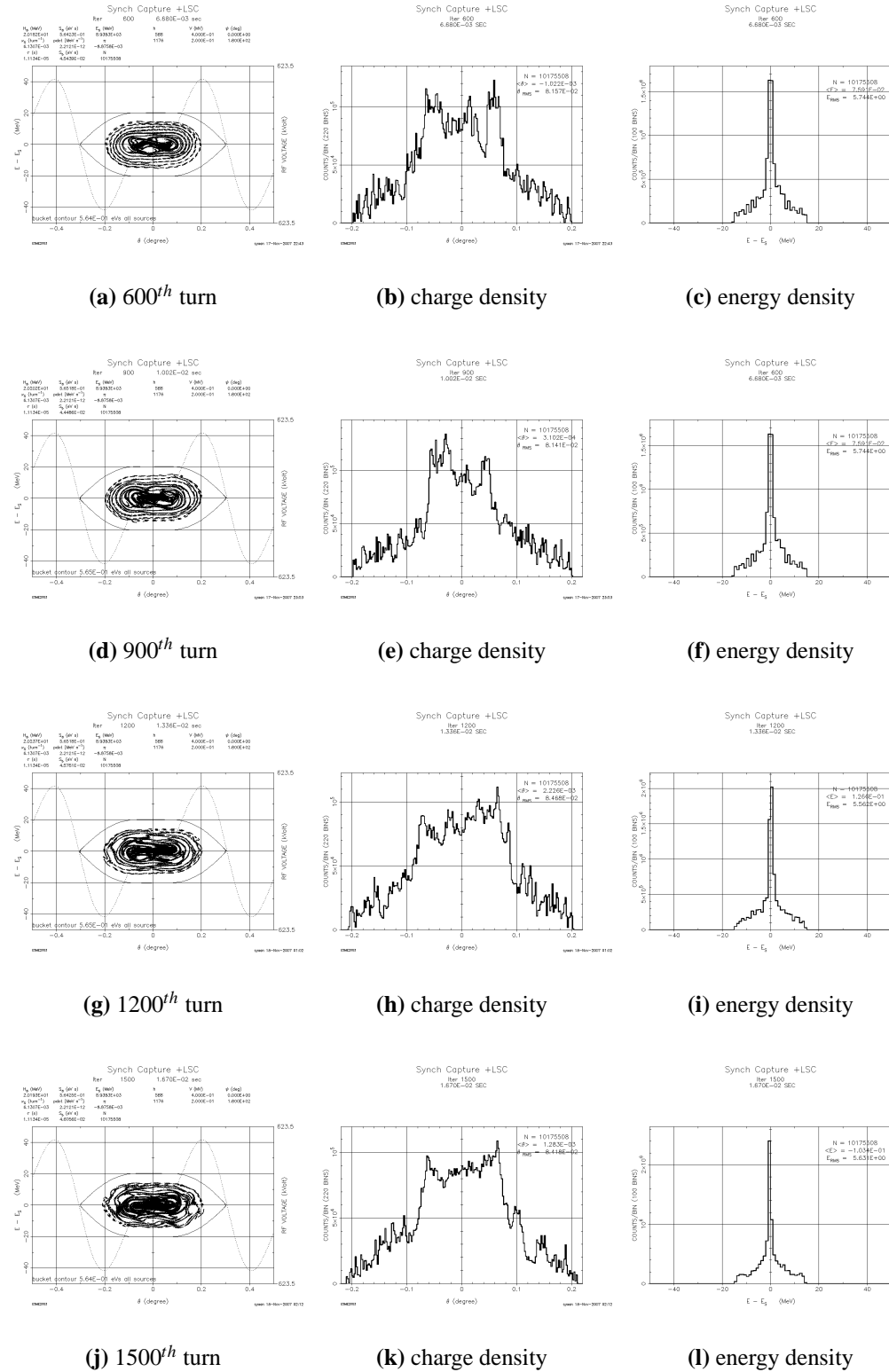


Figure 1.30: [Scenario (IV)] Time evolution of phase space with longitudinal painting starting from 600th turn through 1500th turns

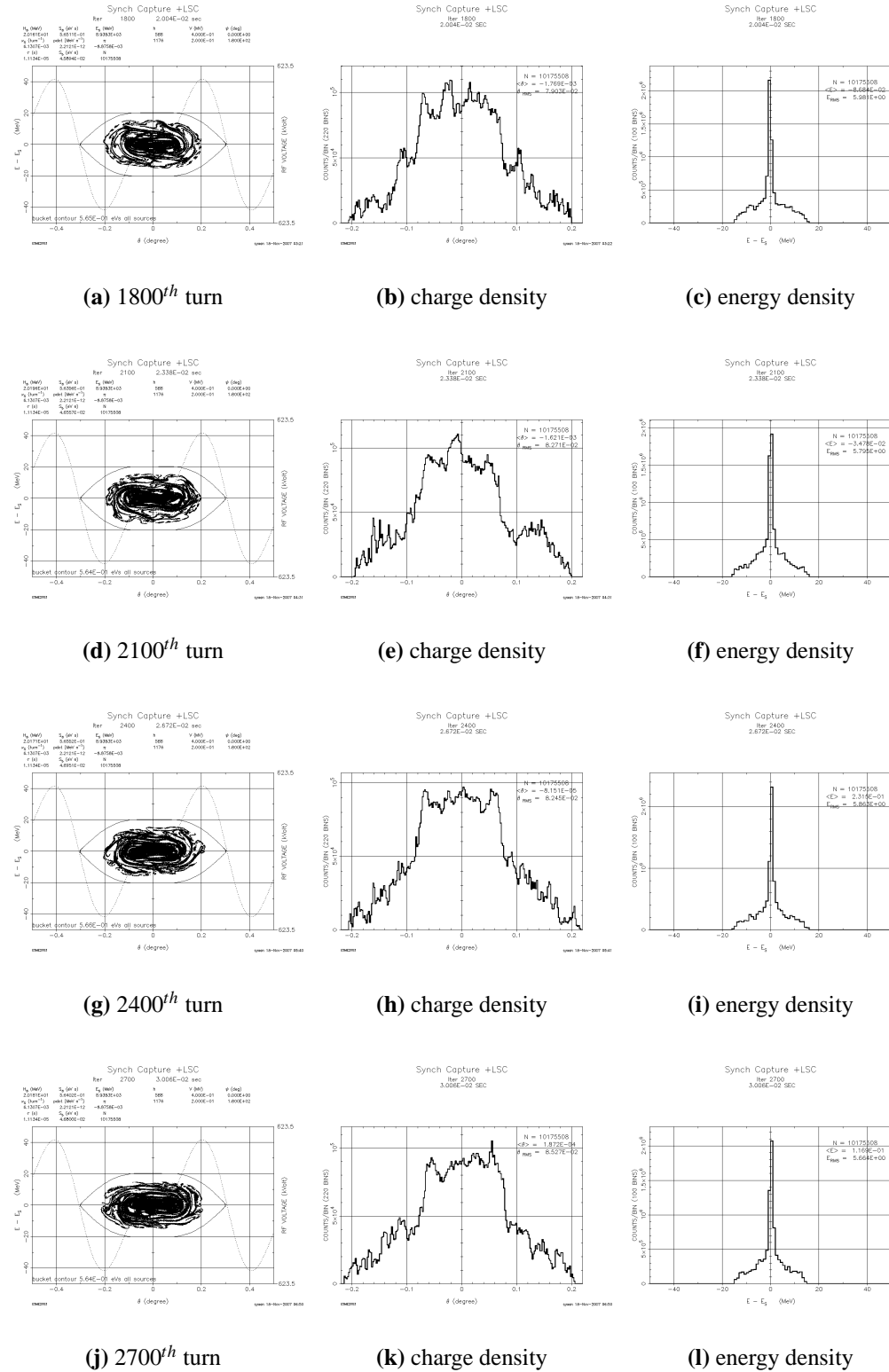


Figure 1.31: [Scenario (IV)] Time evolution of phase space with longitudinal painting starting from 1,800th turn through 2,700th turns

As Figure 1.32 shows, the encouraging result is obtained with the dual RF harmonic system. The longitudinal emittance grows about 50 % less than in the cases of a single RF harmonic system. The peak induced voltage ($\hat{\mathcal{V}}_{sc}$) due to space charge is around 40 (kV) per turn as in Figure 1.33. Figure 1.34 shows the evolution of peak voltage induced by space charge. By using the phase modulation in a controlled fashion, which will allow us to maneuver charge distribution, we will be able to lower space-charge voltage further. The bunching factor calculated at each turn for Scenario (IV) turns out to be close to that of Scenario (I) with a single RF harmonic as in Figure 1.35. It should be noted that the bunching factor calculations are important in that it serves as an indicator of how large tune spreads will be prior to 3-D space-charge calculations.

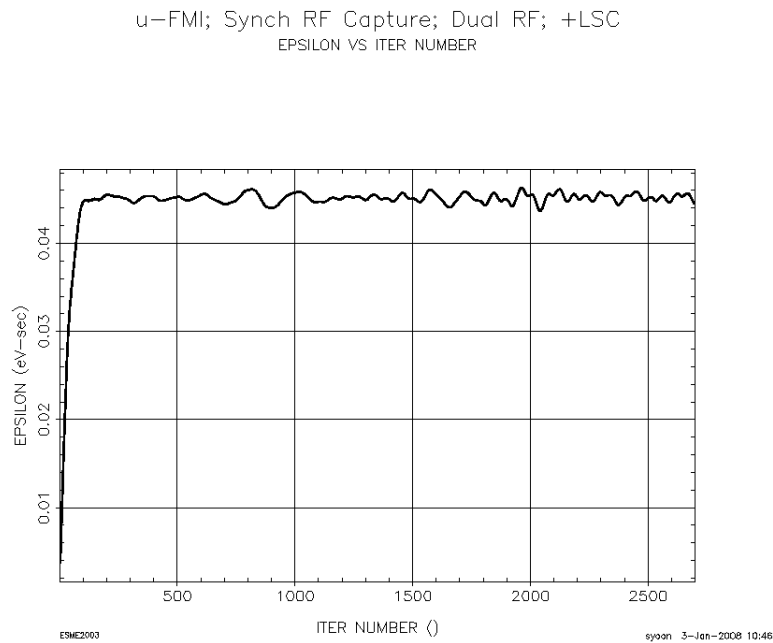


Figure 1.32: [Scenario (IV)] The growth of longitudinal emittance with a dual RF system over 2,700 turns

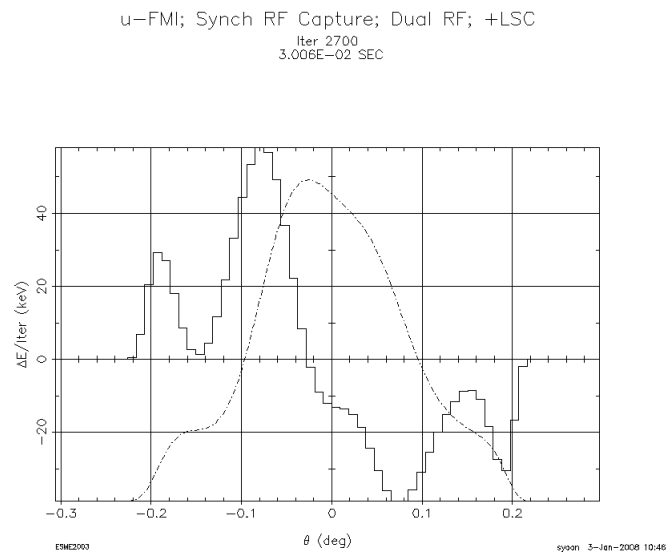


Figure 1.33: [Scenario (IV)] Additional ΔE induced by longitudinal space charge with a dual RF harmonics after 2,700 turns

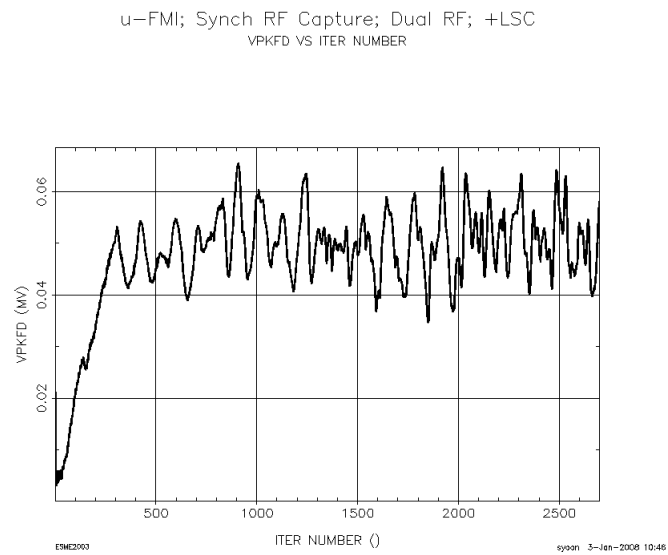


Figure 1.34: [Scenario (IV)] Evolution of peak voltage in frequency domain with a dual RF harmonics over 2,700 turns

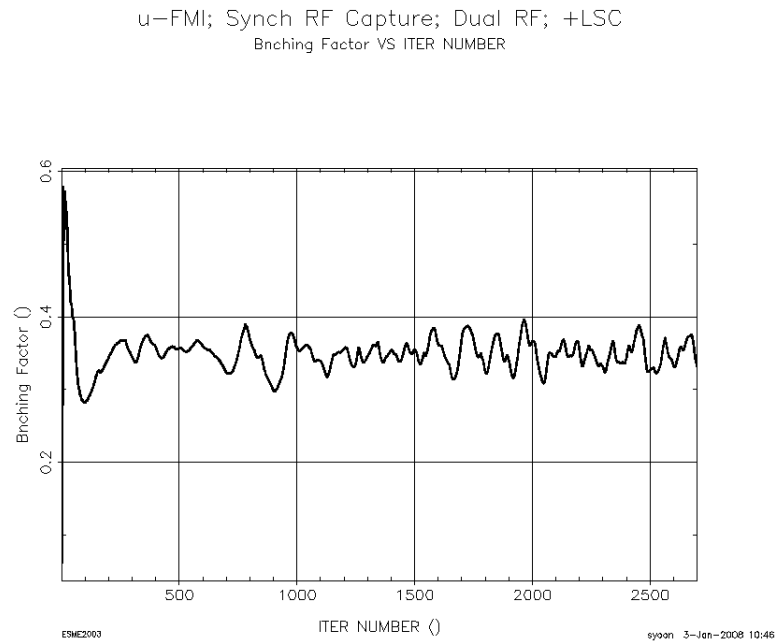


Figure 1.35: [Scenario (IV)] Evolution of bunching factor with a dual RF system

Concluding Remarks

We have investigated different scenarios of microbunch injection-methods between a SC linac and the MI ring under the influence of longitudinal space charge: *from the 8-GeV linac proton driver to the Main Injector*. The RF mismatch between a linac and a ring can induce phase shifts with trains of microbunches, which serve as longitudinal painting in a parasitic fashion. Hence, it would be rather advantageous to use harmonics of *non-integer* ratio between a linac and a ring. In addition to painting in phase, future simulations are planned to include both phase and energy jitters due to errors in the SC RF linac. Because of the short bunch length of the linac beam, it is anticipated that the impact of the broadband impedance may play an important role in the longitudinal dynamics [12]. An optimized dual RF system and longitudinal painting can overcome beam-intensity limitations induced by space charge in high-intensity machines. Four injection scenarios manifest that a double RF system with the harmonic ratio ($\mathcal{R}_H = 1176/588$) of 2.0 and the voltage ratio

($\mathcal{R}_V = 200kV/400kV$) of 0.5 are most favored. All of the scenarios for the time-structured multiturn injection including animated simulation results can be found on a Fermilab web site [13].

Acknowledgement

Authors wish to thank J. Maclachlan of the Proton Source Department and J-P. Carneiro of Accelerator Physics Center (APC) at Fermilab. Authors had useful discussions with J. Maclachlan for an early phase of MI injection modeling with *macrobunches*. J-P. Carneiro provided us with an input file of linac distribution that were generated from the *TRACK* code [7].

Bibliography

- [1] P. S. Yoon, Chapter 7, Ph.D. dissertation, 2007
- [2] G. W. Foster and J. A. MacLachlan, *A multi-mission 8-GeV Injector Linac as a Fermilab Booster Replacement*, Proceedings of LINAC 2002, Gyeongju, Korea, p. 826.
- [3] G. W. Foster, *An 8-GeV Superconducting Injector Linac*, Proceedings of PAC 2005, Knoxville, TN
- [4] G. W. Foster ed., *An 8-GeV SCRF Linac Proton Driver Technical Design Study*, <http://protondriver.fnal.gov/#TechnicalDesignLink> version 56-1, Nov. 2005.
- [5] Agenda for the H^- Transport and Injection Mini-Workshop, December 9-10, 2004, Fermilab, <http://www-bd.fnal.gov/pdriver/H-workshop/>
- [6] D. E. Johnson, P. S. Yoon, C-J Liaw, D. Raperia, and J. Beebee-Wang
An 8-GeV H^- Multi-turn Injection System for the Fermilab Main Injector Proc. of PAC 2007, Albuquerque, NM; Fermilab-Conf-07-287-AD
- [7] P. N. Ostroumov, *Physics Design of the 8-GeV H^- Linac*, New Journal of Physics vol. 8 No.11 [November2006] p. 281,

- [8] R. Madrak, *Fast Beam Chopper for MEBT in the High Intensity Neutrino Source*
Fermilab Beams-Doc 2901, April 2007
- [9] J. A. MacLachlan, *Multiparticle Dynamics in the E- Φ Tracking Code ESME*,
Fermilab-Conf-02/102, 2002
- [10] J. A. MacLachlan, *Presentation at the Proton Driver meeting*, 2005
- [11] P. S. Yoon, *Presentation at the Proton Driver meeting*, 2005
- [12] G. P. Jackson, *Impact of Microwave Impedance in Proton Driver Beams during Synchrotron Injection*, 34th ICFA Advanced Beam Dynamics Workshop on High Power Superconducting Ion, Proton, and Multispecies Ions, Naperville, IL May 2005
- [13] P. S. Yoon, <http://www-ap.fnal.gov/~syoon/SC/FMI.html>